Neuron, Volume *110*

Supplemental information

Walking strides direct rapid and flexible recruitment of visual circuits for course control in *Drosophila*

Terufumi Fujiwara, Margarida Brotas, and M. Eugenia Chiappe

Figure S1 (related to Figure 1): HS cells but not VS cells contribute to steering

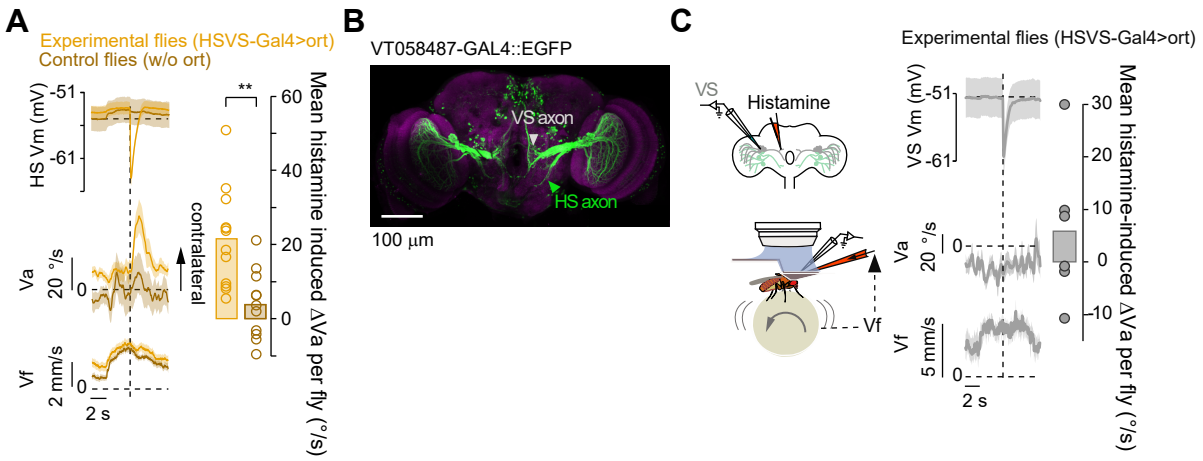

Figure S1 (related to Figure 1): HS but not VS cells contribute to steering. (**A**) Left, Vm, Va, and Vf traces (grand mean ± SEM) in experimental (orange, n=12 flies) or control flies (without exogenous Ort expression, maroon, n=11 flies) triggered at histamine application. Right, mean histamine-induced change in Va (ΔVa) per fly in experimental vs. control flies (p=0.0023, Z=3.05, Wilcoxon rank-sum test). Note that Vm is reported for a subset of flies in which the whole-cell condition lasted until the end of the experiment (7/12 and 6/11 fly-cell pairs for experimental and control flies, respectively). (**B**) Confocal image stack of the VT058487 line driving the expression of EGFP. HS-(green) and VS-cell (light gray) axon terminals are indicated with arrowheads. (**C**) Left, histamine was injected at the axon terminals of VS cells while their activity was monitored by whole-cell patch recordings in flies walking at high speed. Middle, Vm, Va, and Vf triggered at histamine application (n=6 flies, grand mean ± SEM). Note that Vm is reported only for recordings that lasted until the end of the experiment (5/6 fly-cell pairs). Right, mean histamine-induced ΔVa per fly (before injection: -25.8±6.8 °/s vs. after injection: -20.0±8.1 °/s, p=0.69, Wilcoxon signed-rank test, n=6 flies).

Figure S2 (related to Figure 3): Leg movements and their correlation with neural activity and forward velocity

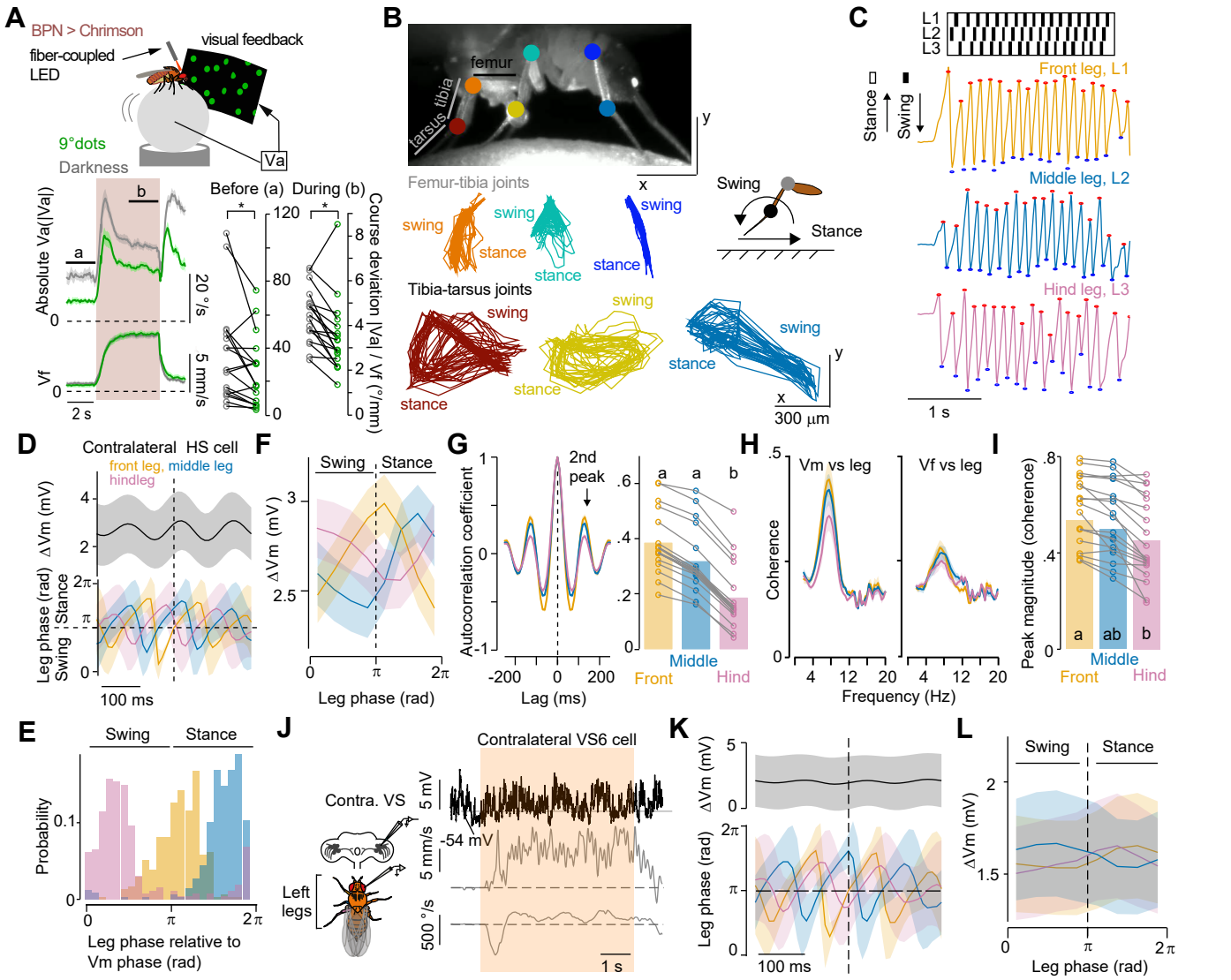

Figure S2 (related to Figure 3): Leg movements and their correlation with neural activity and forward velocity. (**A**) Top, schematic of the experimental closed-loop configuration between the fly's Va and the visual stimuli ("visual feedback", bright green random dots of size 9°, see **STAR Methods**). Bottom, the absolute Va (top, |Va|) and Vf (middle) velocity of flies walking in darkness (gray) or in the presence of visual feedback (green, grand mean ± SEM, n=18 flies). The shaded area indicates the period of optogenetic activation of BPNs, the black line shows the time used for analysis: before (a) and during (b) optogenetic stimulation. Right, mean course deviation, |Va|/Vf, before and during activation of BPNs (black bar) in flies walking in darkness (black) or under the presence of visual feedback (green) (before activation: p=0.016, Z=2.42; during activation: p=0.022, Z=2.29, Wilcoxon signed-rank test). (**B**) Top, side view of an example fly with markers on the femur-tibia and tibia-tarsus joints labeled with DeepLabCut. Bottom, example trajectories of the joints over the stride during a 5s activation of BPNs. Color code indicates the specific leg. (**C**) Top, the swing and stance phases of the three left legs. Bottom, corresponding time courses of the combined x-position of the femur-tibia and tibia-tarsus joints (see **STAR Methods**). Red and blue markers indicate local maxima and minima of the position, corresponding to the onset of swing and stance, respectively. (**D**) Mean ΔVm and leg phases triggered at the stance onset of the left front leg (example fly, n=454 stance onsets). Shaded areas indicate SD. (**E**) Probability distribution of leg phases relative to the phase of Vm oscillations for the example in (**D**). Phase values from 0 to π and from π to 2π correspond to the swing and stance periods of the cycle, respectively. (**F**) HS cells tuning to the contralateral front (orange), middle (blue), and hind (pink) leg movements (grand mean ± SEM, n=19 fly-cell pairs). (**G**) Left, coefficient of autocorrelation of leg movements. Color code: same as in (**B**). Right, amplitude of the coefficient for the second peak in each leg. Letters indicate a significant difference (P<0.05, H=22.56, Kruskal-Wallis followed by Tukey Kramer test, n=19 flies). (**H**) Magnitude-squared coherence between leg movements and Vm (left), and between leg movements and Vf (right) (n=19 fly-cell pairs). (**I**) Magnitude of the coherence peak between leg movement and Vm to each leg (P<0.05, H=6.32, Kruskal-Wallis followed by Tukey Kramer test, n=19 fly-cell pairs). (**J**) Left, schematic of the recorded neural activity and leg movements. Right, example time series of a right VS6 cell's Vm (top), the fly's Vf (middle) and Va (bottom) during activation in BPNs (orange shaded area). (**K**) Mean ΔVm and leg phases triggered at the left front leg's stance onset in the same example. Shaded areas indicate SD (n=775 stance onsets). (**L**) Tuning of contralateral VS cells' Vm to the front (orange), middle (blue), and hind (magenta) leg phases (n=7 fly-cell pairs).

Figure S3 (related to Figure 3): Stride-coupled membrane potential oscillations in HS cells are not induced by activation of BPNs *per se* and reflect actual leg movements

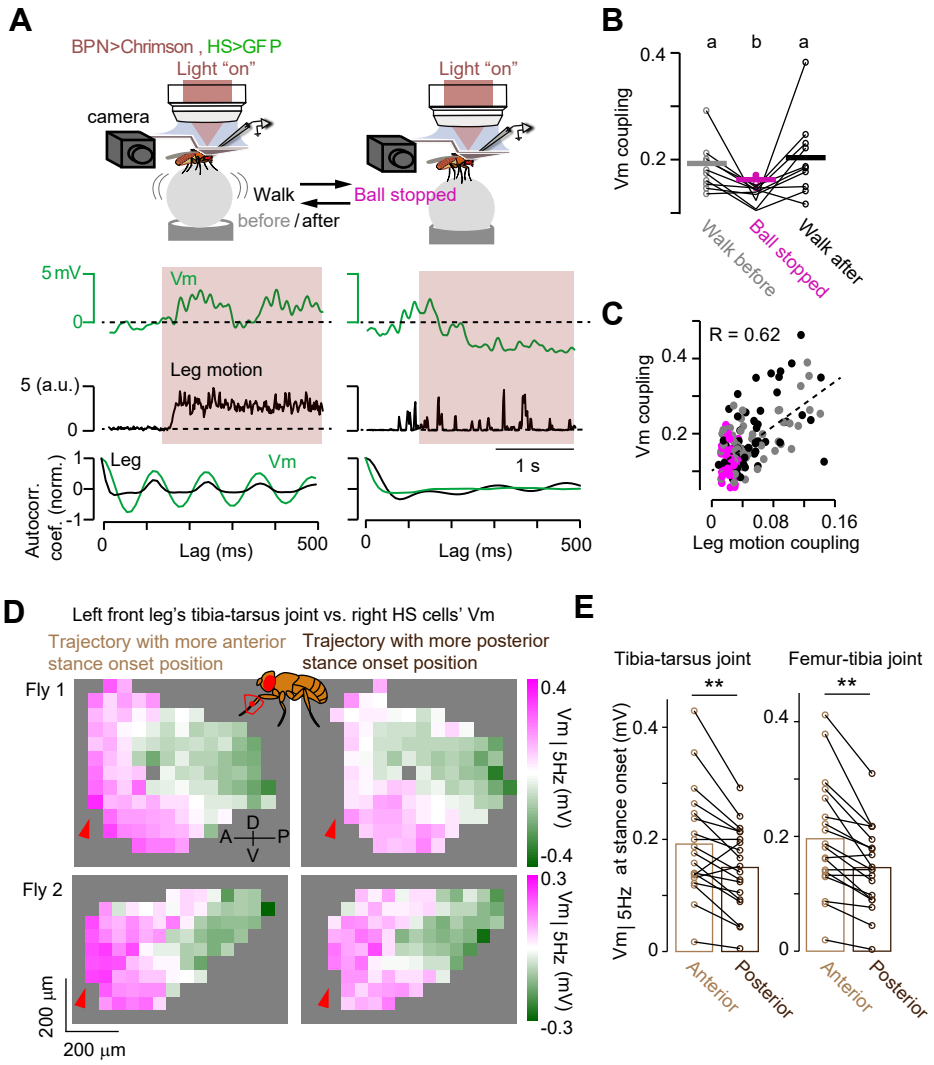

Figure S3 (related to Figure 3): Stride-coupled membrane potential oscillations in HS cells are not induced by activation of BPNs *per se* and reflect actual leg movements. (**A**) Top, schematic of the experimental design. Whole cell-patch recordings from HS cells in simultaneous with optogenetic activation of BPNs (red shadow, "lights on") in walking ("walk", left) or not-walking ("ball stopped", right) flies. The latter condition was induced by stopping the air flow of the ball; note that this manipulation was reversible. To monitor behavior under these conditions, overall leg motion was extracted from the camera tracking legs (see **STAR Methods**). Middle, time series of Vm and the combined leg motion signal. Bottom, normalized autocorrelation coefficient as a function of lag for the neural activity dynamics (Vm, green) and the leg motion signal (leg, black). The oscillatory profile of the autocorrelation for the leg motion signal is characteristic of the periodic nature of walking. (**B**) Quantification of the neural activity autocorrelation strength (Vm coupling) before, during, and after stopping the ball. Letters above the plot indicate significant differences ($p<0.05$, Kruskal-Wallis followed by Tukey Kramer test, $Z=11.34$, $n=10$ fly-cell pairs). (**C**) Correlation between the autocorrelation strength of the fly's leg movements (leg motion coupling) and Vm coupling in each trial. The dashed line shows the linear regression of all the points ($n=180$ trials). (**D**) Left, right HS cells' Vm (high-pass filtered, $Vm_{|5Hz}$) was projected onto a 2D side-view trajectory space for the left front leg's tibia-tarsus joint. Maps were constructed depending on whether the joint position at the stance onset was relatively more anterior (left, distant from the body) or posterior (right, closer to the body). Data from two example flies are shown. Red arrowheads indicate the approximate place of the stance onset. (**E**) Mean $Vm_{|5Hz}$ at the stance onset per fly when the tibia-tarsus (left, $p=0.0022$) or femur-tibia (right, $p=0.00025$, Wilcoxon signed-rank test, $n=19$ fly-cell pairs) joint was placed more anterior (light brown) or posterior (dark brown). A, anterior; D, dorsal; P, posterior; V, ventral.

Figure S4 (related to Figure 3): Simulations incorporating the relation between the forward velocity and HS-cell activity on a rapid timescale support the origin of stride-coupled neural modulations from the contralateral front leg

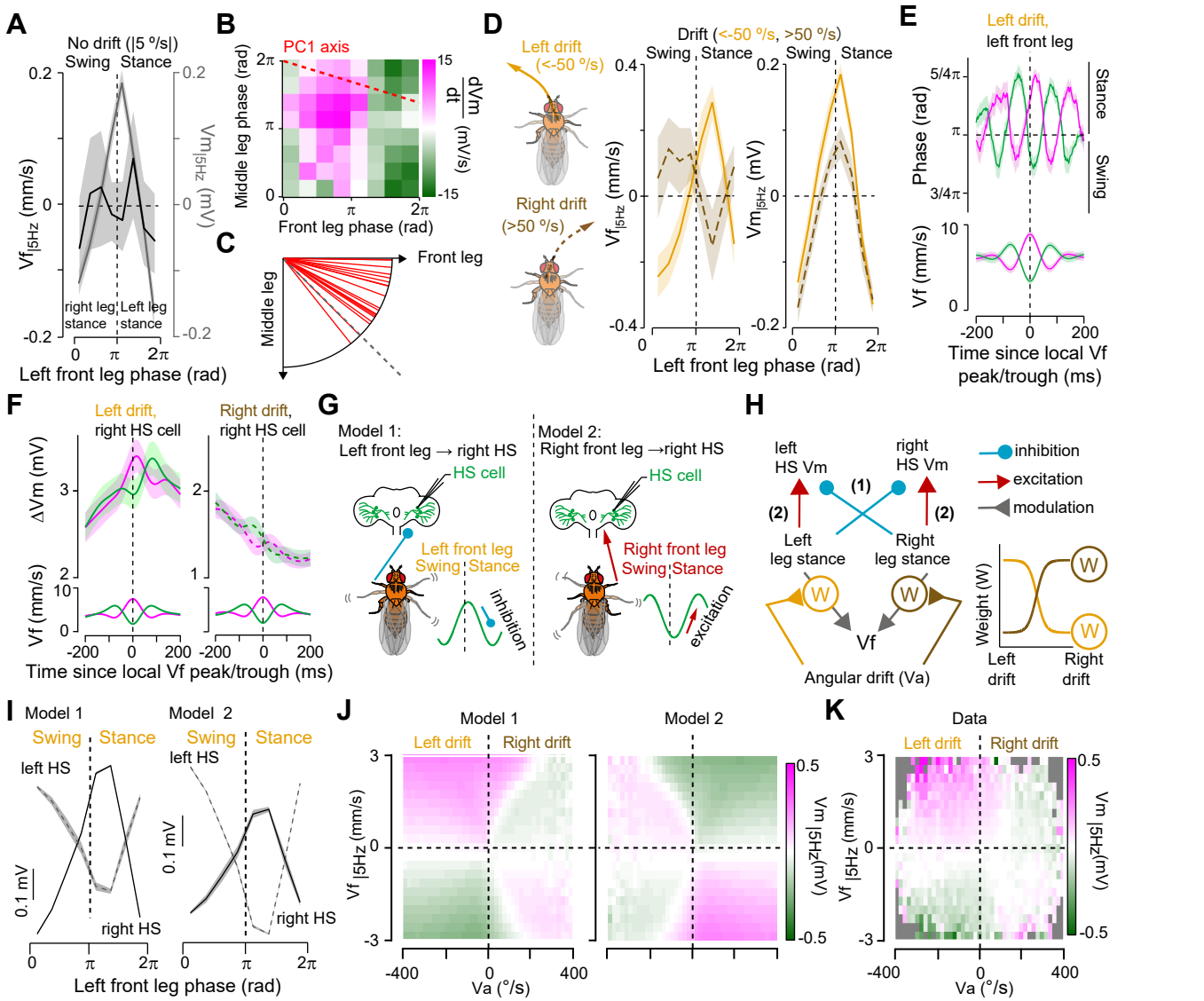

Figure S4 (related to Figure 3): Simulations incorporating the relation between the forward velocity and HS-cell activity on a rapid timescale support the origin of stride-coupled neural modulations from the contralateral front leg. (**A**) Tuning of Vf (high-passed filtered, $Vf_{|5Hz}$) and HS cells (high-passed filtered, $Vm_{|5Hz}$) to the stride cycle of the left front leg during opto-runs with marginal angular drift (-5<Va<5°/s; n=19 fly-cell pairs) (**B**) The temporal derivative of Vm of right HS cells (dVm/dt, from 19 cells) during opto-runs (see **STAR Methods**) projected onto a 2D leg-phase space; x-axis: left front leg, y-axis: left middle leg. The red dashed line indicates the PC1 axis of the 2D map. (**C**) PC1 axis calculated per fly-cell pair (n=19 pairs). The dashed line represents the alignment of the PC1 axis to both the front and middle legs. (**D**) Same as in (**A**) but for opto-runs with left (Va<-50 °/s, orange line) or right (Va>50°/s, maroon dashed line) angular drift (n=18 fly-cell pairs). (**E**) Left front leg phase (top) and Vf (bottom) triggered at the local peak (magenta) or trough (green) of Vf in opto-runs with left angular drift (n=18 fly-cell pairs). (**F**) Change in the activity of HS cells (ΔVm, top) and Vf (bottom) triggered at the local peak (magenta) or through (green) of Vf in spontaneous walking segments with left (n=23 fly-cell pairs, left) or right (n= 24 fly-cell pairs, right) angular drift. (**G**) Two models with different origin for the stride-coupled modulation in HS cells. In model 1, the contralateral front leg drives a hyperpolarizing signal during stance, whereas model 2 proposes a depolarizing drive from the ipsilateral front leg during stance. (**H**) Schematic of the circuit diagram for the simulation. Both right and left legs contributed to Vf with a weight (W) proportional to the ongoing Va, i.e., the direction of the fly's angular drift. (**I**) Simulated tuning of right (solid line) and left (dashed line) HS cells under models 1 (left) and 2 (right). n=50 simulated cells. (**J**) Simulated activity of right HS cells (high-pass filtered, $Vm_{|5Hz}$) as a function of the angular (Va) and forward (high-pass filtered, $Vf_{|5Hz}$) velocities of the fly based on model 1 (left) and model 2 (right). (**K**) Same as (**J**), but actual data (from 25 fly-cell pairs). All the traces show the grand mean ± SEM.

Figure S5 (related to Figure 4). Oscillations in Vm are reduced in flies with perturbed leg mechanosensory activity during periodic walking segments

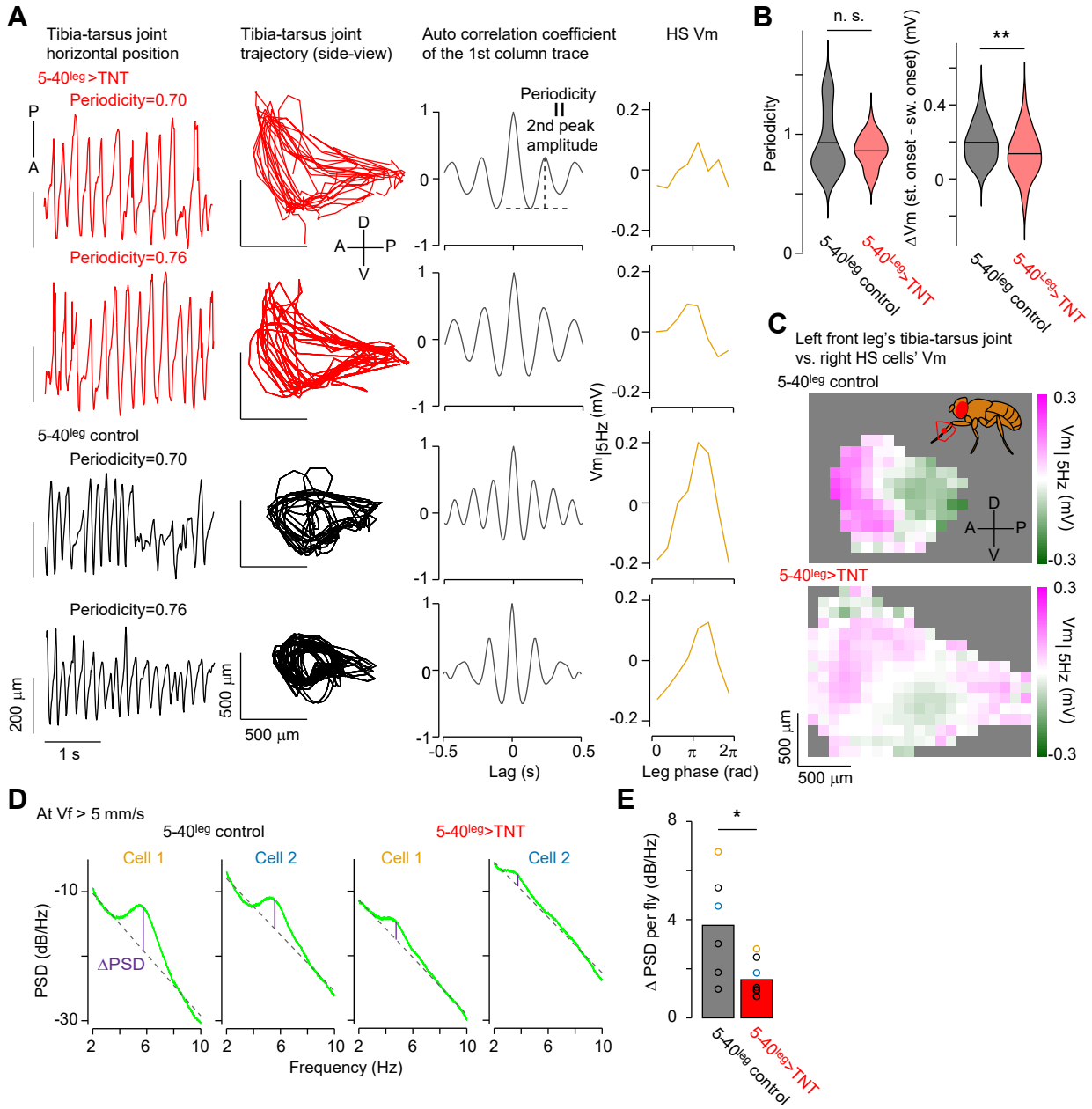

Figure S5 (related to Figure 4). Oscillations in Vm are reduced in flies with perturbed leg mechanosensory activity during periodic walking segments. (**A**) Examples time courses of the horizontal position (1st column) or 2D trajectory (2nd column) of the tibia-tarsus joint side-view trajectories (left front leg), the autocorrelation coefficient of the time series (3rd column), and $Vm_{|5Hz}$ tuning to the leg's stride cycle within the corresponding walking segment (3s, 4th column). Leg movement periodicity was calculated as the second peak amplitude in the autocorrelation coefficient trace. First and 2nd row, experimental flies (red, 5-40^{leg}>TNT); 3rd and 4th row, control flies (black, 5-40^{leg} control). A, anterior; D, dorsal; P, posterior; V, ventral. (**B**) Distributions of periodicity of the leg (left, p=0.62) and change in Vm (ΔVm) between stance and swing onsets (right, $p<10^{-5}$, Wilcoxon rank-sum test, n=208 (5-40^{leg} control, black) vs. n=149 (5-40^{leg}>TNT, red) walking segments. (**C**) Right HS cells' $Vm_{|5Hz}$ in experimental (top) or control (bottom) flies projected onto a 2D side-view trajectory space of the left front leg's tibia-tarsus joint. A, anterior; D, dorsal; P, posterior; V, ventral. (**D**) Power spectral density of Vm when the fly walked at high speed (Vf > 5 mms). Two example cells are shown for control (left) and experimental (right) flies. The strength of stride-related oscillations in Vm was defined as the difference (ΔPSD) between the local peak and the baseline (dashed line) of the PSD plot (see **STAR Methods**). (**E**) ΔPSD was significantly smaller for experimental vs. control flies (p=0.020, Wilcoxon rank-sum test, n=8 (experimental) and n=6 (control) fly-cell pairs).

Figure S6 (related to Figure 5). The excitability of HS cells over a stride strongly correlates with rapid steering independent of the state of angular velocity

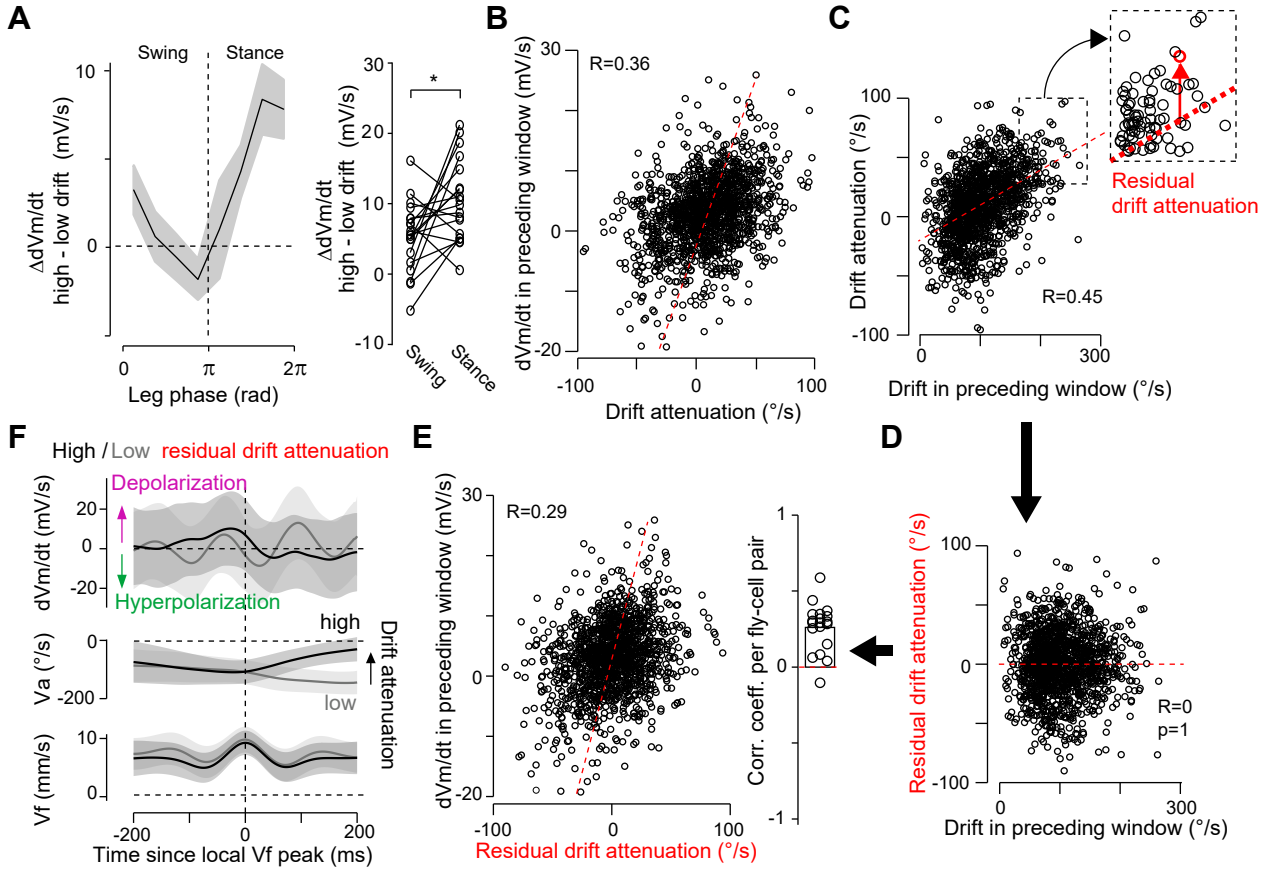

Figure S6 (related to Figure 5). HS-cell activity over a stride correlates with rapid steering independent of the state of angular velocity. (**A**) Left, the difference in HS cells' dVm/dt over a stride cycle of opto-run segments with low (-50°/s <Va<0°/s) vs. high (-200°/s<Va<-150°/s) angular drifts (ΔdVm/dt, see **Figure 5C**). Right, mean ΔdVm/dt per fly during swing vs. stance. Same individual connected by a line. The trace and shaded area represent the grand mean ± SEM, respectively (p=0.020, Z=-2.33, Wilcoxon signed-rank test, n=19 fly-cell pairs). (**B**) Mean temporal derivative of HS cells' membrane potentials (dVm/dt) per opto-run segment before the local Vf peak (time window: 200ms) vs. mean drift attenuation in the following 200ms. The dotted lines indicate the linear regression (R= 0.36, n=1378 segments from 19 fly-cell pairs). (**C**) Mean drift attenuation per opto-run segment over 200ms after the local Vf peak vs. mean angular drift per segment in the preceding 200ms (n=1378 segments from 19 fly-cell pairs). The dotted lines indicate the linear regression (R= 0.45). Inlet: definition of "residual drift attenuation" for an example data point (see also **STAR Methods**). (**D**) Mean residual drift attenuation per opto-run segment vs. the mean preceding angular drift over 200ms before the local Vf peak. The dotted lines indicate the linear regression (by definition, R=0, p=1). (**E**) Mean dVm/dt per opto-run segment over 200ms before the local Vf peak vs. mean residual drift attenuation in the following 200ms. The dotted lines indicate the linear regression (R=0.29). The right panel shows the correlation coefficient per fly-cell pair. The correlation was significantly positive (p=0.00025, z=3.66, Wilcoxon signed-rank test, n=19 fly-cell pairs). (**F**) dVm/dt (top), Va (middle) and Vf (bottom) triggered at the local Vf peak, in opto-run segments with similar magnitude of angular drift before the local Vf peak (leftward direction, Va<-50°/s), but with low (gray) or high (black) residual drift attenuation 200ms after the local Vf peak (n=360 segments; mean ± SD, segments were collected from 19 fly-cell pairs).

Figure S7 (related to Figure 7): Anatomy of LAL-PS-AN$_{contra}$, a class of ascending neurons projecting to IPS and LAL

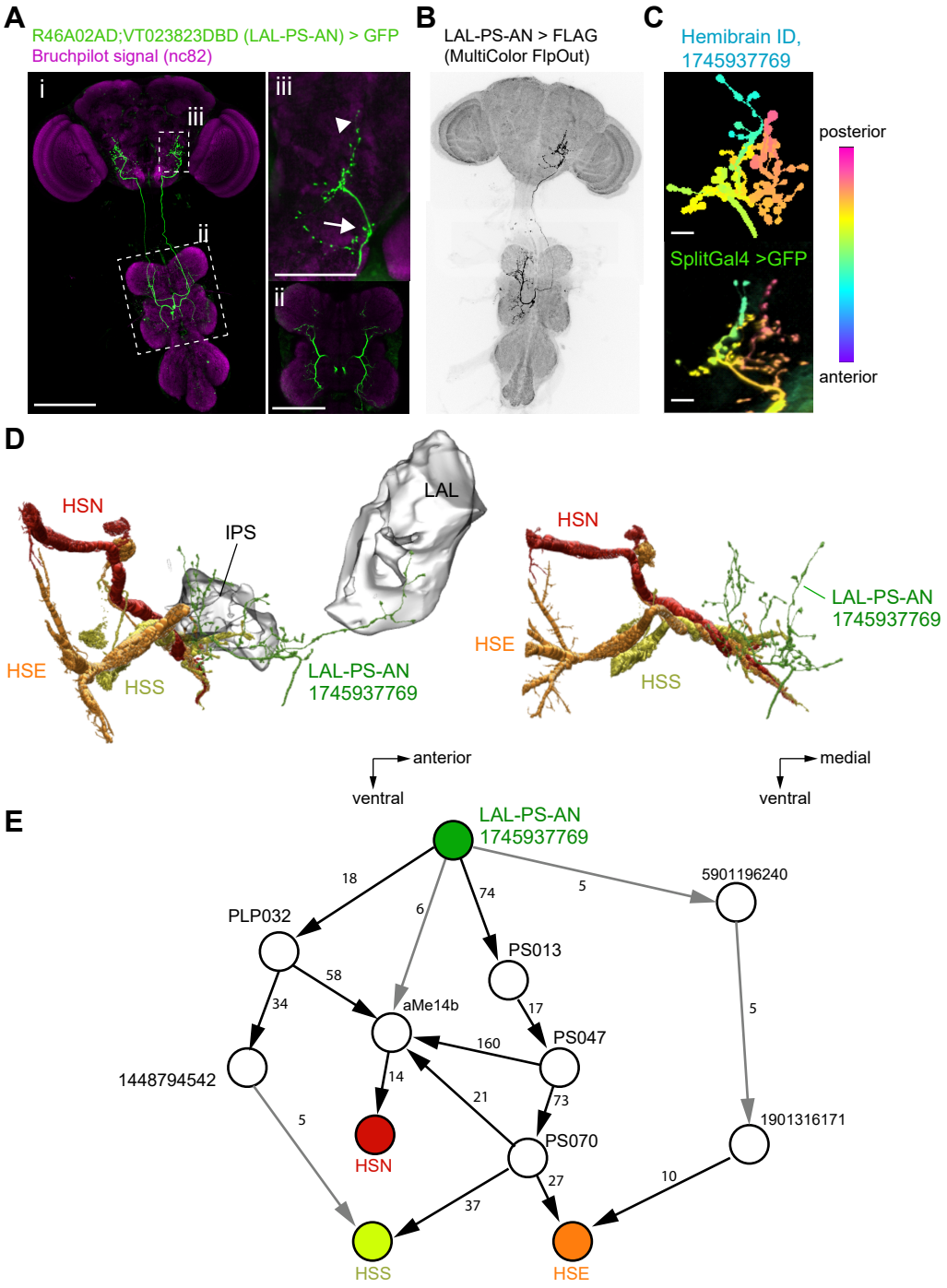

Figure S7 (related to Figure 7): Anatomy of LAL-PS-AN$_{contra}$, a class of ascending neurons projecting to IPS and LAL. (**A**) Projected z-stacked confocal image of the split-GAL4 line R46A02AD-VT023823DBD driving expression of EGFP (i). This line labels a class of ascending neurons that innervates leg neuropil within the proto- and mesomeres of the VNC (ii), and with brain projection fields within the gnathal ganglia (GNG), inferior posterior slope (IPS, arrow), and lateral accessory lobe (LAL, arrowhead) regions (iii). (**B**) A multi-color flip-out image revealing the contralateral projections of an individual LAL-PS-AN$_{contra}$. (**C**) Maximum intensity projection images (MIPs) of an aligned confocal image of our split-GAL4 (bottom) and a putative corresponding neuron identified in the hemibrain EM dataset. Color represents different frames of the image stack in the antero-posterior axis. (**D**) EM-based reconstructed HS cells and the putative LAL-PS-AN$_{contra}$ neuron (green) from the hemibrain dataset (see **STAR Methods**). (**E**) Shortest possible path between the putative LAL-PS-AN$_{contra}$ neuron and HS cells. Synaptic weights: ≥5 synaptic contacts, gray; ≥10 synaptic contacts, black. Scale bars: 100 µm (**A, B**); 10µm (**C**).

Figure S8 (related to Figure 8): Relationship among the stance duration, forward velocity, and left HS-cell activity

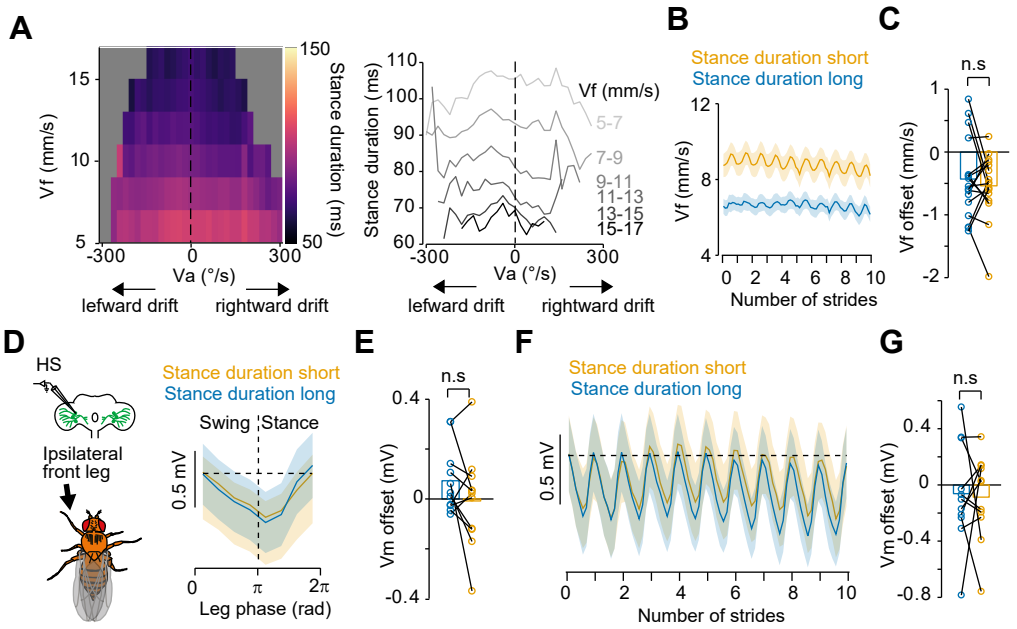

Figure S8 (related to Figure 8): Relationship among the stance duration, forward velocity, and left HS-cell activity. (**A**) Left, front leg stance duration as a function of the angular (x-axis, Va, 20 °/s bins) and forward (y-axis, Vf, 2 mm/s bins) velocities of the fly. Right, the mean stance duration as a function of Va at different Vf. Data were collected from 19 flies. (**B**) Vf tuning to the left front leg stride cycle over ten strides for shorter (orange) or longer (blue) stance duration (grand mean ± SEM, n=17 flies). (**C**) The Vf offset at the end of ten strides relative to the beginning for shorter and longer stance durations (p=0.62, Z=0.50, n=17 flies, Wilcoxon signed-rank test). (**D**) Left, schematic of the experimental configuration. Right, left HS cells tuning to the left front leg phase for shorter (orange) or longer (blue) stance durations (grand mean ± SEM, n=11 fly-cell pairs). (**E**) The Vm offset at the end relative to the beginning of the stride for shorter and longer stance durations (n=11 fly-cell pairs, p=0.28, Wilcoxon signed-rank test). (**F**) Same as (**E**), but traces over ten strides. (**G**) Same as in (**E**) but for ten consecutive strides (p=0.97, n=11 fly-cell pairs, Wilcoxon signed-rank test).